Eur. Phys. J. C 54, 149–158 (2008)
DOI 10.1140/epjc/s10052-007-0505-2

THE EUROPEAN PHYSICAL JOURNAL C

Regular Article – Theoretical Physics

Probing little Higgs model in $e^+e^- \to \nu\bar{\nu}\gamma$ process

T. Aliev[1,a], O. Çakır[2,b]

[1] Middle East Technical University, Faculty of Arts and Science, Department of Physics, Ankara, Turkey
[2] Ankara University, Faculty of Sciences, Department of Physics, 06100, Tandogan, Ankara, Turkey

Received: 15 September 2007 /
Published online: 9 January 2008 –

Abstract. We study the process $e^+e^- \to \nu\bar{\nu}\gamma$ to search for its sensitivity to the extra gauge bosons Z_2, Z_3 and $W_2^{\pm}$, which are suggested by the little Higgs models. We find that the ILC with $\sqrt{s} = 0.5$ TeV and CLIC with $\sqrt{s} = 3$ TeV cover different regions of the LHM parameters. We show that this channel can provide a determination of the parameters, complementary to measurements of the extra gauge bosons obtainable at the upcoming LHC experiments.

PACS. 14.80.Cp; 12.60.Fr; 12.60.Cn

1 Introduction

Despite the impressive success of the standard model (SM) in describing all existing experimental data at currently available energies, it contains many unsolved problems. For example, the origin of the fermion mass, the origin of the CP violation, hierarchy problems, etc. Therefore, it is commonly believed that SM is a low energy manifestation of a more fundamental theory. In order to solve the hierarchy and fine-tuning problems between the electroweak scale and the Planck scale, new physics at the TeV scale is expected. In coming years the large hadron collider (LHC) and later the international linear collider (ILC) will provide us detailed information about the electroweak symmetry breaking and the origin of the hierarchy of fermion masses and CP-violating interactions. Supersymmetry introduces an extended space-time symmetry and removes the quadratically divergent corrections due to the superpartners of fermions and bosons. Extra dimensions reinterpret the problem completely by lowering the fundamental Planck scale. Technicolor theories introduce new strong dynamics at a scale not much above the electroweak scale, and thus defer the hierarchy problem. Among the most popular non-supersymmetric model for solving the hierarchy problem is the so-called little Higgs model [1–5] (and references therein). It is expected that the global symmetry breaking scale should be $\lesssim 10$ TeV in order for the little Higgs model to be relevant for the hierarchy. The little Higgs model solves the problem at one-loop level by eliminating the quadratic divergencies via the presence of a partially broken global symmetry SU(5). The masses of these gauge bosons are expected to be of the order of the global symmetry breaking scale f for $\mathrm{SU}(5) \to \mathrm{SO}(5)$. In other words, the new heavy particles in this model cancel the quadratic divergencies in question. The subgroup $[\mathrm{SU}(2) \times \mathrm{U}(1)]^2$ is also broken into the $\mathrm{SU}(2)_{\mathrm{L}} \times \mathrm{U}(1)_Y$ group of the SM at the scale f of a few TeV and then $\mathrm{U}(1)_{\mathrm{em}}$ at the Fermi scale $v \simeq 246$ GeV. The minimal type is the 'littlest Higgs model' (LHM), in addition to the SM particles, new charged heavy vector bosons $W_2^{\pm}$ (or heavy $W_{\mathrm{H}}^{\pm}$), two neutral vector bosons Z_2 (or heavy Z_{H}) and Z_3 (or a heavy photon A_{H}), a heavy top quark (T) and a triplet of scalar heavy particles ($\phi^{\pm}, \phi^0$) are present.

Since the LHM predicts many new particles, the search of these particles usually is performed in two different ways: i) via their indirect effects, i.e. these particles new at loop and change SM predictions on flavor changing neutral current processes (FCNC), ii) their direct productions in high energy colliders.

The relevant scale f of new physics must be $\gtrsim 2$–3 TeV in order to be consistent with the electroweak precision data [6–21]. A consequence of the littlest Higgs model in rare FCNC B and K decays has comprehensively been studied in [12–16]. This channel was studied previously, but not for the LHM, in [22] to examine the sensitivity to the extra gauge bosons Z' and W' predicted by various extensions of the SM. Recently, an analysis of the sensitivity to the neutrino couplings of the neutral gauge bosons and to the couplings of the extra charged gauge boson has been made by [21]. Direct productions of new particles in high energy colliders are discussed in [17–20]. The direct production of new heavy gauge bosons are kinematically limited by the available center of mass energy of the present colliders. At the large hadron collider (LHC), the possible signals of extra gauge bosons would show up through peaks in the invariant mass distributions of their decay products [23].

[a] e-mail: taliev@metu.edu.tr
[b] e-mail: ocakir@science.ankara.edu.tr

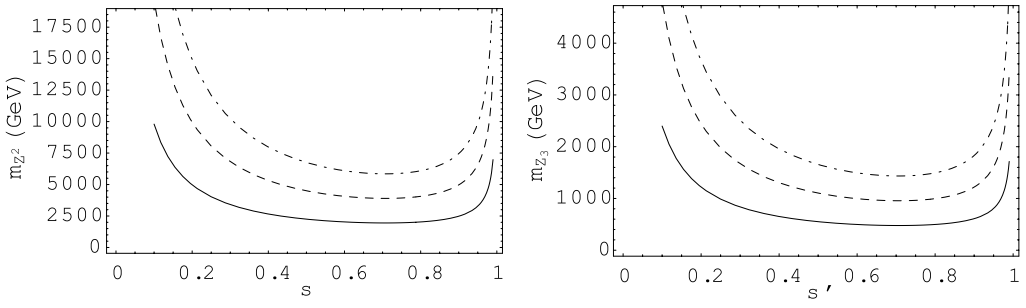

Fig. 1. Heavy gauge boson masses m_{Z_2} (*left*) and m_{Z_3} (*right*), depending on the mixing s (where $s' = 0.5$) and s' (where $s = 0.5$) for the various scales $f = 3\,\text{TeV}$ (*solid line*), $f = 6\,\text{TeV}$ (*dashed line*) and $f = 9\,\text{TeV}$ (*dot-dashed line*)

In the present work, we study the indirect effects of extra gauge bosons in the cross sections of the process $e^+e^- \to \nu\bar{\nu}\gamma$ at high energy linear e^+e^- colliders; namely, the international linear collider (ILC) [24, 25][1] and the compact linear collider (CLIC) [27–30]. In addition to the limits from hadron colliders, an improvement on the sensitivity of the physical observables will be reached at future e^+e^- linear colliders. This study can be considered as complementary to [21, 22]. Finally, we give an analysis of the LHM parameters that will be measurable at the ILC and CLIC.

2 Theoretical framework

The process $e^+e^- \to \nu\bar{\nu}\gamma$ is widely discussed in connection to the determination of the number of neutrinos [31] and the understanding dynamics of stellar processes. Before the discussion of the $e^+e^- \to \nu\bar{\nu}\gamma$ process in the LHM, a few illuminating remarks about main ingredients of the LHM are in order. In the little Higgs model in addition to the standard $W^\pm$ and Z boson contributions there are contributions coming from new heavy vector bosons, i.e. from the extended gauge sector. The kinetic term of the scalar field Σ in the lagrangian has the form [1, 2]

$$L = \frac{f^2}{8}\,\mathrm{Tr}\,|D_\mu \Sigma|^2\,, \tag{1}$$

with the covariant derivative of the scalar Σ field

$$D_\mu \Sigma = \partial_\mu \Sigma - \mathrm{i}\sum_{k=1}^{2}\left[g_k\left(W_k\Sigma + \Sigma W_k^{\mathrm{T}}\right) + g_k'\left(B_k\Sigma + \Sigma B_k^{\mathrm{T}}\right)\right], \tag{2}$$

where g_k and g_k' are the coupling constants related to the gauge fields W_k and B_k. The mixing angles s and s', $s = g_2/\sqrt{g_1^2 + g_2^2}$ and $s' = g_2'/\sqrt{g_1'^2 + g_2'^2}$ relate the coupling strengths of the two $\mathrm{SU}(2) \times \mathrm{U}(1)$ gauge groups. The relations between the gauge bosons in weak and mass eigenstates are similar to the SM case; namely

$$\begin{pmatrix} W \\ W' \end{pmatrix} = \begin{pmatrix} s & c \\ -c & s \end{pmatrix}\begin{pmatrix} W_1 \\ W_2 \end{pmatrix}, \quad \begin{pmatrix} B \\ B' \end{pmatrix} = \begin{pmatrix} s' & c' \\ -c' & s' \end{pmatrix}\begin{pmatrix} B_1 \\ B_2 \end{pmatrix}, \tag{3}$$

where W and B are the gauge boson states associated with the generators of SU(2) and U(1) of the SM. W' and B' are the massive gauge bosons with masses $m_{W'} = gf/2sc$ and $m_{B'} = g'f/2\sqrt{5}s'c'$. Here $s, s'(c, c')$ represent the sine (cosine) of the two mixing angles. After electroweak symmetry breaking all the light and heavy gauge bosons are obtained, and these include Z_1, $W_1^\pm$ and γ of the SM and $W_2^\pm$, Z_2 and Z_3 of the LHM.

The masses of the new heavy gauge bosons in the LHM to the order of $\mathcal{O}(v^2/f^2)$ are given by the following expressions [3–5]:

$$m_{Z_1} = m_Z\left[1 - \frac{v^2}{f^2}\left(\frac{1}{6} + \frac{1}{4}(c^2 - s^2)^2 + \frac{5}{4}(c'^2 - s'^2)^2 + 8\frac{v'^2}{v^2}\right)\right]^{1/2}, \tag{4}$$

$$m_{Z_2} = m_W\left(\frac{f^2}{s^2c^2v^2} - 1 - \frac{x_{\mathrm{H}}s_W^2}{s'^2c'^2c_W^2}\right)^{1/2}, \tag{5}$$

$$m_{Z_3} = m_Z s_W\left(\frac{f^2}{5s'^2c'^2v^2} - 1 + \frac{x_{\mathrm{H}}c_W^2}{4s^2c^2s_W^2}\right)^{1/2}, \tag{6}$$

$$m_{W_1} = m_W\left[1 - \frac{v^2}{f^2}\left(\frac{1}{6} + \frac{1}{4}(c^2 - s^2)^2\right) + 4\frac{v'^2}{v^2}\right]^{1/2}, \tag{7}$$

$$m_{W_2} = m_W\left(\frac{f^2}{s^2c^2v^2} - 1\right)^{1/2}, \tag{8}$$

where m_Z and m_W are the SM gauge boson masses and c_{W} (s_{W}) denotes the cosine (sine) of the Weinberg weak mixing angle. Here x_{H} characterizes the mixing between B' and W' in the Z_2 and Z_3 eigenstates and it depends on the gauge couplings. As can be seen from Fig. 1, the mass of the new neutral gauge boson Z_2 (Z_3) strongly depends on s (s'). The mass of the heavy gauge boson $W_2^\pm$ depends on the scale f and the mixing s, and for the ratio $m_{Z_2}/m_{W_2} \simeq 1$ holds for the region of interest. The charged gauge boson mass m_{W_2} can be approximated as the left panel in Fig. 1. From (5) and (6) we obtain the ratio satisfying $m_{Z_3}/m_{Z_2} \simeq 0.25$ for some ranges of the parameters s and s'. Figure 1 reflects this property and the mass of the Z_3 boson remains below 1 TeV for a wide range of the parameter s'. We may note that Z_3 is much lighter than Z_2 and could be searched for at ILC energies. If ILC does not discover the Z_3 boson it is possible to put a lower bound on the scale, $f \gtrsim 3\,\text{TeV}$.

[1] Comprehensive information about the future linear colliders can be found in [26].

The coupling between neutral gauge bosons (Z_i) and fermions can be written in the form $-\mathrm{i}\gamma^\mu(g_\mathrm{V}+g_\mathrm{A}\gamma^5)$, and the charged gauge bosons ($W_i^\pm$) have the couplings of type $-\mathrm{i}g_W(1-\gamma^5)$ with the leptons in the framework of the LHM. The couplings g_V and g_A also depend on the mixing parameter s, s' and the scale f, while g_W depends on s and f. The expressions for these couplings are given in Table 1. In order to see how the $Z_1e^+e^-$ vector and axial-vector couplings change from their SM values we give a 3D plot in Fig. 2. We find that the relative changes in g_V are much greater than for g_A for the values of s' near the endpoints. It is possible to set a bound on s and s' by demanding these couplings to remain perturbative, and hence one obtains the limit $s, s' > 0.1$. As can be seen from Table 1, the $Z_3l\bar{l}$ coupling vanishes for $c' = \sqrt{2/5}$ once given $y_e = 0.6$.

The couplings of the Z_1 boson and the W_1 boson to the SM leptons are subject to corrections in the LHM. We calculate the relative changes in g_W for the values of s and f as shown in Fig. 3. There are only little changes in g_W for small values of f. As can be seen from Table 1 the coupling for $W_2^\pm$ reduces to the SM coupling for $W_1^\pm$ for $s^2 = c^2 = 0.5$. Using their couplings as shown in Table 1 one obtains for the Z_1 total decay width and W_1 boson mass up to corrections proportional to $\mathcal{O}(v^2/f^2)$: $\Gamma_{Z_1} \simeq \Gamma_Z(1+1.7v^2/f^2)$ and $m_{W_1} \simeq m_W(1+0.89v^2/f^2)$, leading to the comment that $f > 8\,\mathrm{TeV}$ even for small c'. Since there are some partial cancellations, in fact, as a general guide we take $v/f \lesssim 0.1$. In Table 2 we present the total decay

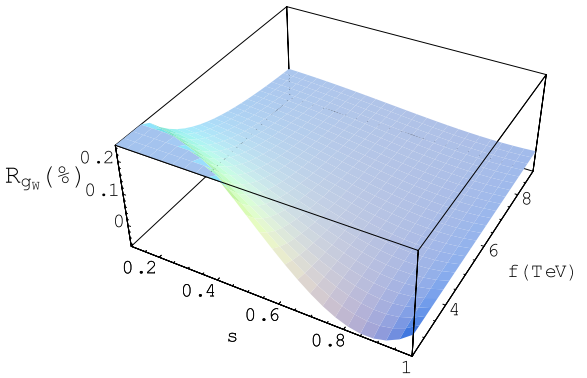

Fig. 3. The relative change R_{g_W} (%) of the $W_1^+e^-\bar{\nu}_e$ couplings from the SM values depending on s and f

Table 1. Neutral and charged gauge boson–fermion couplings in the little Higgs model. The last line denotes the $W^+_{1(2)}W^-_{1(2)}\gamma$ couplings

Particles	g_V	g_A
$Z_1\nu\bar{\nu}$	$\frac{g}{2c_\mathrm{W}}\left\{\frac{1}{2}-\frac{v^2}{f^2}\left[c_\mathrm{W}x_Z^{W'}\frac{c}{2s}+\frac{s_\mathrm{W}x_Z^{B'}}{s'c'}\left(y_e-\frac{4}{5}+\frac{c'^2}{2}\right)\right]\right\}$	$-g_\mathrm{V}$
$Z_2\nu\bar{\nu}$	$gc/(4s)$	$-g_\mathrm{V}$
$Z_3\nu\bar{\nu}$	$\frac{g'}{2s'c'}\left(y_e-\frac{4}{5}+\frac{c'^2}{2}\right)$	$-g_\mathrm{V}$
$Z_1e^-e^+$	$\frac{g}{2c_\mathrm{W}}\left\{-\frac{1}{2}+2s_\mathrm{W}^2-\frac{v^2}{f^2}\left[-c_\mathrm{W}x_Z^{W'}\frac{c}{2s}+\frac{s_\mathrm{W}x_Z^{B'}}{s'c'}\left(2y_e-\frac{9}{5}+\frac{3c'^2}{2}\right)\right]\right\}$	$\frac{g}{2c_\mathrm{W}}\left\{\frac{1}{2}-\frac{v^2}{f^2}\left[c_\mathrm{W}x_Z^{W'}\frac{c}{2s}+\frac{s_\mathrm{W}x_Z^{B'}}{s'c'}\left(-\frac{1}{5}+\frac{c'^2}{2}\right)\right]\right\}$
$Z_2e^-e^+$	$-gc/(4s)$	$-g_\mathrm{V}$
$Z_3e^-e^+$	$\frac{g'}{2s'c'}\left(2y_e-\frac{9}{5}+\frac{3c'^2}{2}\right)$	$\frac{g'}{2s'c'}\left(-\frac{1}{5}+\frac{c'^2}{2}\right)$
	Coupling g_W	
$W_1^+e^-\bar{\nu}$	$\frac{g}{2\sqrt{2}}\left[1-\frac{v^2}{2f^2}c^2(c^2-s^2)\right]$	
$W_2^+e^-\bar{\nu}$	$-\frac{g}{2\sqrt{2}}\frac{c}{s}\left[1+\frac{v^2}{2f^2}s^2(c^2-s^2)\right]$	

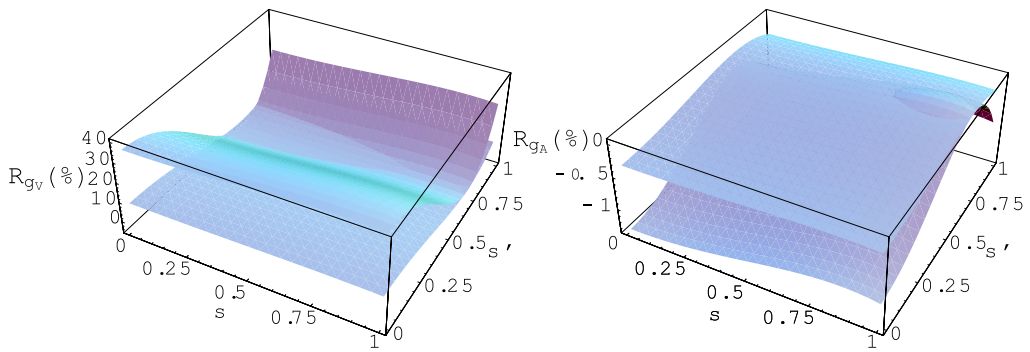

Fig. 2. The relative changes R_{g_V} (%) and R_{g_A} (%) of the $Z_1e^+e^-$ vector g_V and axial-vector g_A couplings from the SM values depending on s and s', taking the scale $f = 3\,\mathrm{TeV}$ (*upper on first panel*, *lower on second panel*) and $f = 6\,\mathrm{TeV}$ (*lower on first panel*, *upper on second panel*)

Table 2. Masses and decay widths of the neutral ($Z_{2,3}$) and charged ($W_2^{\pm}$) gauge bosons. Here we use $v/f = 0.1$ and $y_e = 0.6$

$\sin\theta/\sin\theta'$	m_{Z_2} (GeV)	m_{Z_3} (GeV)	m_{W_2} (GeV)	Γ_{Z_2} (GeV)	Γ_{Z_3} (GeV)	Γ_{W_2} (GeV)
0.1/0.1	8034.4	1971.2	8034.4	27153.0	6614.7	26899.80
0.3/0.1	2787.0	1971.7	2792.4	960.32	693.95	953.17
0.4/0.1	2138.4	1972.7	2179.6	382.35	370.61	385.61
0.5/0.3	1843.9	684.5	1844.8	187.99	70.06	186.09
0.5/0.5	1844.5	451.7	1844.8	188.05	45.90	186.09
0.5/0.9	1844.1	499.6	1844.8	188.01	50.84	186.09
0.9/0.5	2036.2	452.6	2036.6	17.95	3.65	17.78
0.9/0.9	2036.3	498.7	2036.6	17.95	4.09	17.78

widths of the Z_2, Z_3 and $W_2^{\pm}$ bosons, which we need in the calculation of the cross section for the process $e^+e^- \to \nu\bar{\nu}\gamma$. The decay of the heavy gauge boson Z_2 includes the leptonic, hadronic and gauge boson channels to give the partial widths of the form [3–5]

$$\begin{aligned}
\Gamma(Z_2 \to l^+l^-) &\simeq \frac{g^2\cot^2\theta}{96\pi} m_{Z_2}\,,\\
\Gamma(Z_2 \to \bar{q}q) &\simeq \frac{g^2\cot^2\theta}{32\pi} m_{Z_2}\,,\\
\Gamma(Z_2 \to Z_1 h) &\simeq \frac{g^2\cot^2 2\theta}{192\pi} m_{Z_2}\,,\\
\Gamma(Z_2 \to W_1^+W_1^-) &\simeq \frac{g^2\cot^2 2\theta}{192\pi} m_{Z_2}\,, \qquad (9)
\end{aligned}$$

where we neglect the corrections from the v/f terms and the final state masses. The partial decay widths for the $W_2^{\pm}$ bosons can be obtained from (9) using isospin symmetry, as follows:

$$\begin{aligned}
\Gamma(W_2^{\pm} \to l^{\pm}\nu) &\simeq \frac{g^2\cot^2\theta}{48\pi} m_{W_2}\,,\\
\Gamma(W_2^{\pm} \to \bar{q}'q) &\simeq \frac{g^2\cot^2\theta}{16\pi} m_{W_2}\,,\\
\Gamma(W_2^{\pm} \to W_1^{\pm}h) &\simeq \frac{g^2\cot^2 2\theta}{192\pi} m_{Z_2}\,,\\
\Gamma(W_2^{\pm} \to W_1^{\pm}Z_1) &\simeq \frac{g^2\cot^2 2\theta}{192\pi} m_{Z_2}\,. \qquad (10)
\end{aligned}$$

The gauge boson Z_3 is assumed to be light and could be explored at future colliders. Similarly, its decay width can be obtained from (1) by replacing $g \to g'$ and $\theta \to \theta'$.

After these preliminary remarks, let we consider the process $e^-(p_1)e^+(p_2) \to \nu(k_1)\bar{\nu}(k_2)\gamma(k)$ in LHM, for which the relevant diagrams are presented in Fig. 4. In the SM, this process proceeds via s-channel Z and t-channel $W^{\pm}$ exchange with the photon being radiated from the initial charged particles. In the LHM models this process has also contributions from both s-channel Z_2, Z_3 and t-channel $W_2^{\pm}$ exchange. We implement all relevant vertices in the CalcHEP [32, 33] in the framework of the littlest Higgs model. The amplitudes for the diagrams Fig. 4a–c are given by

$$\begin{aligned}
M_1 = \sum_{a=1}^{3} &\bar{u}(k_1)\left[-\mathrm{i}\gamma^{\mu}\left(g_{\mathrm{V}}^{a(\nu)} + g_{\mathrm{A}}^{a(\nu)}\gamma_5\right)\right]v(k_2)\\
&\times\left[\frac{-\mathrm{i}\left(g_{\mu\nu} - q_{1\mu}q_{1\nu}/m_{Z_a}^2\right)}{q_1^2 - m_{Z_a}^2 + \mathrm{i}m_{Z_a}\Gamma_{Z_a}}\right]\bar{v}(p_2)(\mathrm{i}g_e\not{\varepsilon})\left[\frac{\mathrm{i}(\not{q}+m_e)}{q^2-m_e^2}\right]\\
&\times(-\mathrm{i}\gamma^{\nu})\left(g_{\mathrm{V}}^{a(e)} + g_{\mathrm{A}}^{a(e)}\gamma_5\right)u(p_1)\,, \qquad (11)
\end{aligned}$$

where $q_1 = k_1 + k_2$, $q = k - p_2$ and ε_μ is the photon polarisation four-vector. The amplitudes for Fig. 4d–f are given by

$$\begin{aligned}
M_2 = \sum_{a=1}^{3} &\bar{u}(k_1)\left[-\mathrm{i}\gamma^{\mu}\left(g_{\mathrm{V}}^{a(\nu)} + g_{\mathrm{A}}^{a(\nu)}\gamma_5\right)\right]v(k_2)\\
&\times\left[\frac{-\mathrm{i}\left(g_{\mu\nu} - q_{1\mu}q_{1\nu}/m_{Z_a}^2\right)}{q_1^2 - m_{Z_a}^2 + \mathrm{i}m_{Z_a}\Gamma_{Z_a}}\right]\bar{v}(p_2)(-\mathrm{i}\gamma^{\nu})\\
&\times\left(g_{\mathrm{V}}^{a(e)} + g_{\mathrm{A}}^{a(e)}\gamma_5\right)\left[\frac{\mathrm{i}(\not{q}'+m)}{q'^2-m_e^2}\right](\mathrm{i}g_e\not{\varepsilon})u(p_1)\,,
\end{aligned} \qquad (12)$$

where $q' = p_1 - k$. The amplitudes for Fig. 4g and h are given by

$$\begin{aligned}
M_3 = \sum_{b=1}^{2} &\bar{u}(k_1)\left(-\mathrm{i}g_{\mathrm{V}}^{b}\gamma^{\mu}\right)(1-\gamma_5)\left[\frac{\mathrm{i}(\not{q}+m_e)}{q'^2-m_e^2}\right](\mathrm{i}g_e\not{\varepsilon})u(p_1)\\
&\times\left[\frac{-\mathrm{i}\left(g_{\mu\nu} - q_{3\mu}q_{3\nu}/m_{W_b}^2\right)}{q_3^2 - m_{W_b}^2 + \mathrm{i}m_{W_b}\Gamma_{W_b}}\right]\\
&\times\bar{v}(p_2)\left(-\mathrm{i}g_{\mathrm{V}}^{b}\gamma^{\nu}\right)(1-\gamma_5)v(k_2)\,, \qquad (13)
\end{aligned}$$

where $q_3 = p_2 - k_2$. The amplitudes for Fig. 4i and j are given by

$$\begin{aligned}
M_4 = \sum_{b=1}^{2} &\bar{u}(k_1)\left(-\mathrm{i}g_{\mathrm{V}}^{b}\gamma^{\mu}\right)(1-\gamma_5)u(p_1)\\
&\times\left[\frac{-\mathrm{i}\left(g_{\mu\nu} - q_{4\mu}q_{4\nu}/m_{W_b}^2\right)}{q_4^2 - m_{W_b}^2 + \mathrm{i}m_{W_b}\Gamma_{W_b}}\right]\\
&\times\bar{v}(p_2)(\mathrm{i}g_e\not{\varepsilon})\left[\frac{\mathrm{i}(\not{q}+m)}{q^2-m_e^2}\right]\left(-\mathrm{i}g_{\mathrm{V}}^{b}\gamma^{\nu}\right)(1-\gamma_5)v(k_2)\,,
\end{aligned} \qquad (14)$$

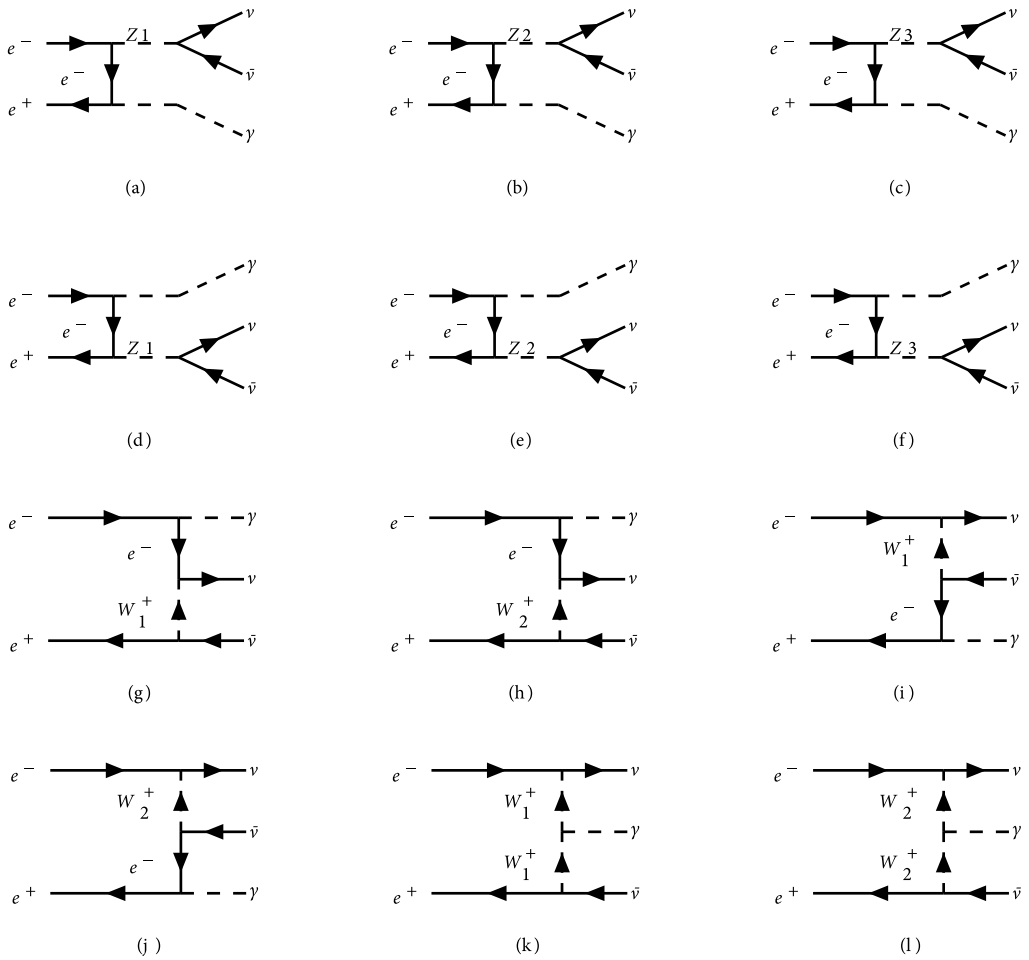

Fig. 4. The Feynman diagrams contributing to the process $e^+e^- \to \nu\bar{\nu}\gamma$

where $q_4 = k_1 - p_1$. The amplitudes for Fig. 4k and l are given by

$$
\begin{aligned}
M_5 = \sum_{b=1}^{2} & \bar{u}(k_1)\big(-\mathrm{i}g_{\mathrm{V}}^{b}\gamma_\mu\big)(1-\gamma_5)u(p_1) \\
& \times \left[\frac{-\mathrm{i}\big(g^{\mu\mu'} - q_4^{\mu}q_4^{\mu'}/m_{W_b}^2\big)}{q_4^2 - m_{W_b}^2 + \mathrm{i}m_{W_b}\Gamma_{W_b}}\right] \\
& \times \mathrm{i}g_e\big[g_{\nu'\lambda}(q_3+k)_{\mu'} + g_{\lambda\mu'}(-k+q_4)_{\nu'} \\
& + g_{\mu'\nu'}(-q_4-q_3)_{\lambda}\big]\varepsilon^{\lambda}\left[\frac{-\mathrm{i}\big(g^{\nu\nu'} - q_3^{\nu}q_3^{\nu'}/m_{W_b}^2\big)}{q_3^2 - m_{W_b}^2 + \mathrm{i}m_{W_b}\Gamma_{W_b}}\right] \\
& \times \bar{v}(p_2)\big(-\mathrm{i}g_{\mathrm{V}}^{b}\gamma_\nu\big)(1-\gamma_5)v(k_2)\,. \qquad (15)
\end{aligned}
$$

3 Numerical results

We will be interested in the differential cross sections over the kinematic observables of the photon energy E_γ and its angle relative to the incident electron direction, respectively. The double differential cross section of the considered process is given by

$$
\frac{\mathrm{d}\sigma}{\mathrm{d}E_\gamma\,\mathrm{d}\cos\theta_\gamma} = \frac{|M|^2 E_\gamma}{128\pi^3 s}\,, \qquad (16)
$$

where the amplitude M is the sum of the above five amplitudes, $M_{1\text{–}5}$. In order to remove the collinear singularities, when the photon is emitted in the initial beam direction, we apply the initial kinematic cuts: $E_\gamma > 10\,\mathrm{GeV}$ and $10^\circ < \theta_{e\gamma} < 170^\circ$. We may also impose a cut, $p_{\mathrm{T}\gamma} > 10\,\mathrm{GeV}$, on the transverse momentum of photon to remove the large background from radiative Bhabba scattering. Figure 5 shows the total cross section for $e^+e^- \to \nu\bar{\nu}\gamma$ as a function of the center of mass energy $\sqrt{s}$ for the SM and two different values of the LHM parameters s and s'. Starting from a center of mass energy just greater than the Z mass, a minimum around $\sqrt{s} \simeq 300\,\mathrm{GeV}$ occurs due to the SM Z boson resonance tail on the high energies. For different values of the parameters s, s' and f the shape of the LHM curves changes, leading to the appearance/disappearance of the resonance peaks. For the proposed energies and luminosities of the ILC and CLIC e^+e^- colliders we can well measure different extra gauge boson couplings for the region of interest of the parameters. In other words, preferably we may search for the parameters for Z_3 at ILC

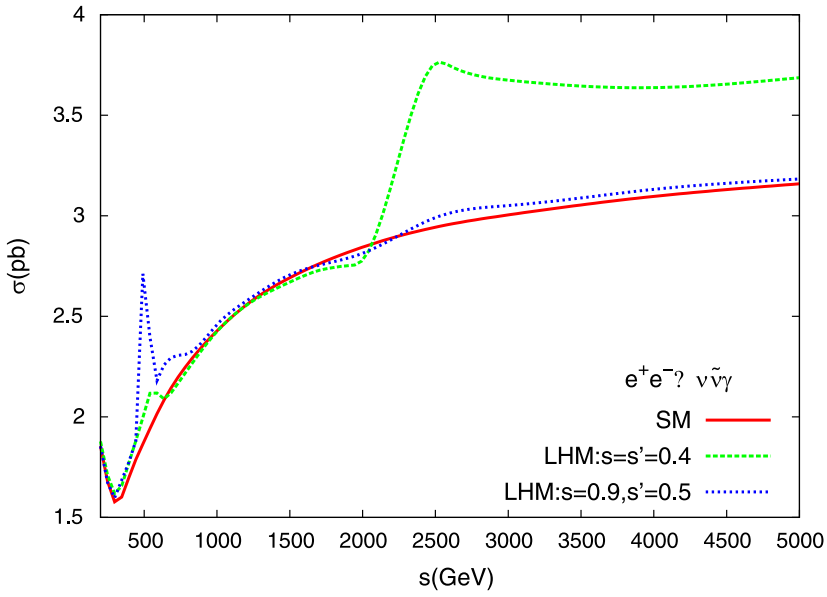

Fig. 5. The total cross section in pb versus center of mass energy $\sqrt{s}$. For the LHM model we take two different points for s, s' and $v/f = 0.1$

(0.5–1 TeV) energies and the parameters for Z_2 at CLIC energies (1–5 TeV). The charged new heavy gauge boson $W_2^{\pm}$ contributes to the total cross section slightly but its presence in the t-channel shows no resonance behavior. Since the heavy charged boson ($W_2^{\pm}$) couplings depend on the mixing parameter s and the scale f, for a certain scale the s parameter determination will include the admixture of the heavy gauge bosons, while the s' determination from the Z_2 contribution can only be done by choosing a specific value in which the Z_3 decouples from the process.

In Tables 3 and 4 we present the total cross section for the process $e^+e^- \to \nu\bar{\nu}\gamma$ with both signal and SM background. We find that the total cross section (signal plus background) changes at most 44% at $\sqrt{s} = 0.5$ TeV for the region of interest of the parameters s, s' with the scale $f = 2.46$ TeV. There is also a large contribution from the extra gauge bosons, mainly Z_2, for the relatively small parameter $s' = 0.1$ with larger values of $s = 0.9$ and the scale $f = 3.5$ TeV at the center of mass energy $\sqrt{s} = 3$ TeV, as shown in Table 4. In order to see the sensitivity of the photon energy to new physics, in Fig. 6 we plot the differential cross section versus E_γ by taking $v/f = 0.1$ at the center of mass energy $\sqrt{s} = 0.5$ TeV and $\sqrt{s} = 3$ TeV, respectively. We see that for the value of the parameter $s' = 0.5$ the Z_3 resonance occurs as its magnitude strongly depends on the values of s. The peak in the cross section due to the Z_3 (Z_2) boson shifts to the right as s decrease. We see from Fig. 6 that the main contributions to the total cross section (signal plus background) comes from three regions, the low energy region, the resonance region and the region due to radiative return to the Z pole, where $E_\gamma = \sqrt{s}(1 - m_Z^2/s)/2 \approx 240$ GeV. The pole region ($\sim \sqrt{s}/2$) is quite insensitive to the new physics. The resonance region for Z_3 occurs at $s' = 0.5$ and $f \simeq 1$–3 TeV. The peak of the resonance shifts to lower photon energies (left) when the scale f increased as shown in Fig. 7. This is due to the fact that as f increases the extra gauge boson masses ($\propto f$) also increase, and as the resonance occurs there remains a lower energy delivered to the photon, i.e. the lower E_γ, the higher the mass probed in the Z_i propagator via $E_\gamma = \sqrt{s}(1 - m_{Z_i}^2/s)/2$. For a visible signal peak one can scan the parameter f between $\simeq 1$–3 TeV at a collider energy of $\sqrt{s} = 0.5$ TeV. At higher center of mass energies such as $\sqrt{s} = 3$ TeV this resonance scan can be extended to upper values of the scale f around $\simeq 2$–4 TeV.

We calculate the relevant backgrounds from the reactions $e^+e^- \to Z\gamma$ $(2 \to 2)$, which is the part of the $e^+e^- \to$

Table 3. The cross sections (in pb) for $e^+e^- \to \nu\bar{\nu}\gamma$ with $v/f = 0.1$ at $\sqrt{s} = 500$ GeV. The corresponding SM background gives $\sigma_B = 1.879$ pb. Here we applied the minimal cuts $E_\gamma > 10$ GeV, $10^\circ < \theta_{13} < 170^\circ$ and $p_T > 10$ GeV

$\sin\theta \backslash \sin\theta'$	0.1	0.3	0.5	0.7	0.9
0.1	1.9379	1.9347	1.9382	1.9396	1.9384
0.3	1.9662	1.9701	1.9035	1.8919	1.9041
0.5	1.9761	2.0012	1.9294	1.8806	1.9305
0.7	1.9755	1.9983	2.0394	1.8905	1.9583
0.9	1.9606	1.9915	2.7090	1.8878	1.9668

Table 4. The cross sections (in pb) for $e^+e^- \to \nu\bar{\nu}\gamma$ with $v/f = 0.07$ at $\sqrt{s} = 3000$ GeV. The corresponding SM background gives $\sigma_B = 3.013$ pb. Here we applied the minimal cuts $E_\gamma > 10$ GeV, $10^\circ < \theta_{13} < 170^\circ$ and $p_T > 10$ GeV

$\sin\theta \backslash \sin\theta'$	0.1	0.3	0.5	0.7	0.9
0.1	3.2502	3.2093	3.2206	3.2359	3.2311
0.3	4.2023	3.0384	3.0505	3.0578	3.0614
0.5	10.369	3.3954	3.4205	3.4199	3.4083
0.7	24.491	3.1316	3.1323	3.1345	3.1343
0.9	66.303	3.1130	3.0709	3.0768	3.0722

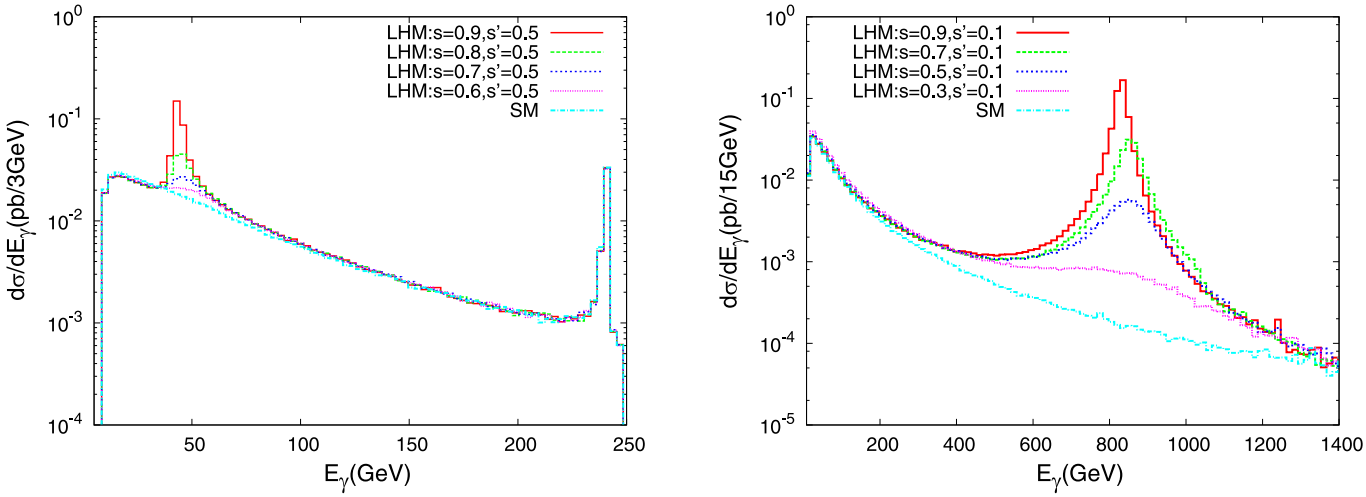

Fig. 6. Differential cross section versus photon energy at $\sqrt{s} = 500$ GeV (*left*) and $\sqrt{s} = 3000$ GeV (*right*) for $v/f = 0.1$ and different values of s, s'

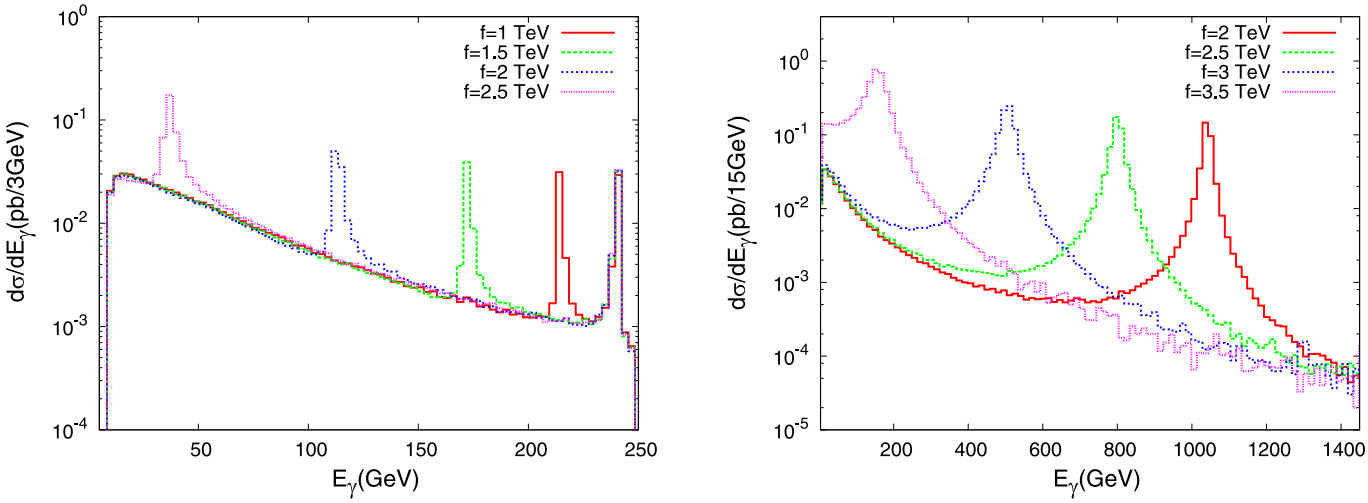

Fig. 7. Energy distribution of photon for various values of the scale f at $\sqrt{s} = 500$ GeV (*left*) and $\sqrt{s} = 3000$ GeV (*right*). The sine of the mixing angle is taken as $s = 0.9$ and $s' = 0.5$ for the *left plot*, and $s = 0.9$ and $s = 0.1$ for the *right plot*

$\nu\bar{\nu}\gamma$ $(2 \to 3)$ reaction, $e^+e^- \to ZZ\gamma$ $(2 \to 3)$ and $e^+e^- \to Z\nu\bar{\nu}\gamma$ $(2 \to 4)$ with (w) and without (o) ISR effects at the ILC and CLIC energies. With the initial cuts we find the background cross sections as shown in Table 5. We see that the main contribution to the background comes from $e^+e^- \to \nu\bar{\nu}\gamma$, which includes both $e^+e^- \to Z\gamma$ $(2 \to 2)$ and $e^+e^- \to \nu\bar{\nu}\gamma$ $(2 \to 3$ with only W_1 exchange). Here we take the branching ratio of $Z^0 \to$ *invisible* decay as 20%. A background that cannot be suppressed comes from the process $e^+e^- \to \nu\bar{\nu}\nu'\bar{\nu}'\gamma$ with a cross section $\sigma \backsimeq 23$ fb. In order to see the photon energy distribution (between the initial cuts and the kinematical cuts) of these backgrounds in the

Table 5. The cross sections (in fb) for relevant background processes at ILC and CLIC energies with (w) and without (o) initial state radiation (ISR) from e^+ and e^- beams. Here, we applied only the initial cuts

w/o ISR	$\sigma(\nu\bar{\nu}\gamma)$	$\sigma(Z\gamma)$	$ZZ\gamma$	$Z\nu\bar{\nu}\gamma$
0.5 TeV	1843.0/1879.3	2273.0/1730.5	22.94/22.71	10.88/11.76
1 TeV	2372.6/2429.5	582.16/416.13	11.96/11.20	35.73/39.92
3 TeV	2970.4/3012.7	70.03/45.72	3.00/2.63	129.72/133.18
5 TeV	3125.4/3152.2	26.43/16.44	1.44/1.23	174.81/189.04

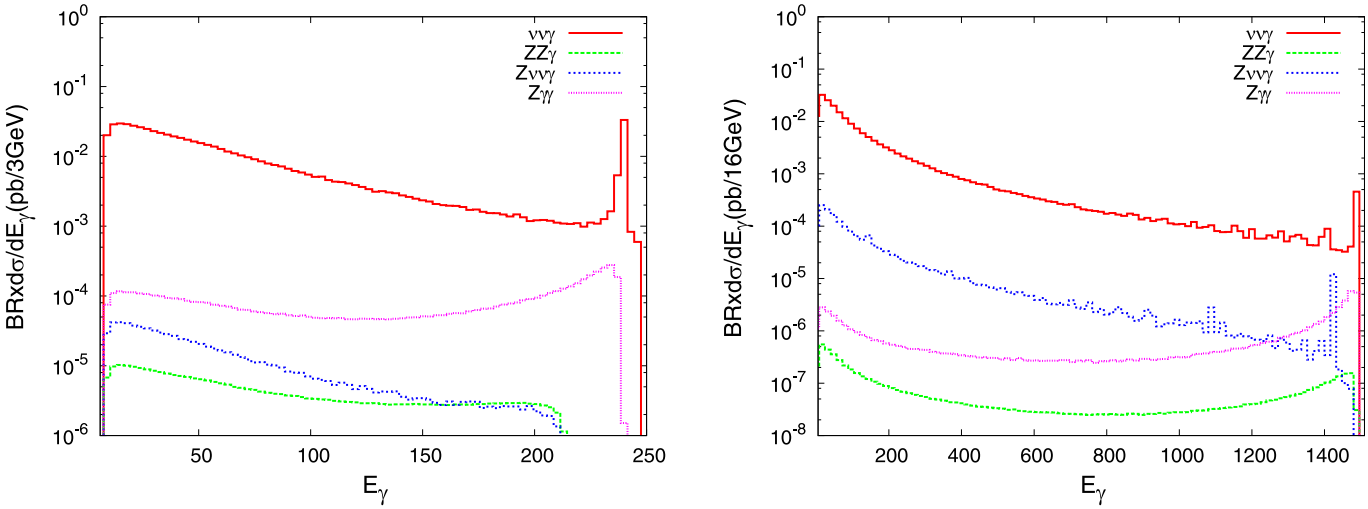

Fig. 8. Backgrounds contributing to the "$\gamma + \not{p}_{\mathrm{T}}$" analysis

"$\gamma + \not{p}_{\mathrm{T}}$" analysis we show differential cross sections multiplied by the corresponding branching ratios in Fig. 8 at the center of mass energies $\sqrt{s} = 0.5$ TeV and $\sqrt{s} = 3$ TeV. Here, we assume lepton universality, and we calculate the cross sections to give an idea about the magnitude of the background considered. In general, applying some strict cuts around the resonance regions and by making an optimization for the ratio S/B, the measurements can also be improved, provided that the LHC measures the masses of the extra gauge bosons predicted by the LHM.

For a given center of mass energy we can determine the contributions from new gauge bosons in different parameter regions: a first one is the resonant region where a peak in the distribution is obtained for certain values of the parameters s, s' and f; a second one is the non-resonant region where the parameter scans can be performed over a wide range; a third one is the decoupling region ($c' = \sqrt{2/5}$) where the coupling of Z_3 to fermions vanishes, and here there is also another approach based on the idea that the mass of the new gauge boson can be taken infinitely heavy. We show the results for the cases mentioned on proceeding with our analysis.

In order to obtain the discovery limits of the LHM parameters we perform a χ^2 analysis. We calculate the χ^2 distribution to be

$$\chi^2 = \sum_{k=1}^{n} \left(\frac{\frac{\mathrm{d}\sigma^k}{\mathrm{d}E_\gamma}(\mathrm{LHM}) - \frac{\mathrm{d}\sigma^k}{\mathrm{d}E_\gamma}(\mathrm{SM})}{\delta \frac{\mathrm{d}\sigma^k}{\mathrm{d}E_\gamma}(\mathrm{SM})} \right)^2 , \qquad (17)$$

where $\delta\, \mathrm{d}\sigma^k/\mathrm{d}E_\gamma$ is the error on the measurement including statistical and systematical errors added in quadrature. As we already noted, the backgrounds are much smaller than the signal, and we expect that the statistical errors in the SM backgrounds would be smaller than the systematic errors including detector and e^-/e^+ beam uncertainties. Here, we considered a systematic error $\delta_{\mathrm{sys}} = 5\%$ for a measurement. This may be an overestimate, however; if improved, the constraints can be relaxed and benefit from the advantage of a high luminosity. The differential cross section depends on the model parameters s, s' and f. We may assume that the LHC would have determined the mass of the extra gauge bosons relatively well. Thus we can fix the masses m_{Z_2}, m_{Z_3} and m_{W_2}, and perform a two-parameter scan. We calculate χ^2 at every point of s, s'. In this case $\chi^2 = \chi^2_{\mathrm{min}} + C$. The constraint on the parameters with 95% C.L. can be obtained at the ILC and CLIC energies by requiring $C = 5.99$ for two free parameters. In calculating the χ^2 for $\mathrm{d}\sigma/\mathrm{d}E_\gamma$ we have used equal sized bins in the range $E_\gamma^{\mathrm{min}} < E_\gamma < E_\gamma^{\mathrm{max}}$, where the upper limit is taken as the kinematical limit for the photon energy. The most sensitive results can be obtained for $s' = 0.5(0.1)$ at the center of mass energy $\sqrt{s} = 0.5(3)$ TeV as shown in Fig. 9. The χ^2_i distributions versus the photon energy bin show peaks shifted to the right depending on lower s and lower f values. Here we have used $v/f = 0.1$ and 0.07 for the ILC and CLIC energies, respectively.

In Fig. 10 we present the constraints on the mixing parameters s, s' in a density plot. For the Z_3 search at the ILC energies with $L_{\mathrm{int}} = 100\,\mathrm{fb}^{-1}$ most of the s, s' parameter space can be discovered. A contour line for the constrained parameter space (s, s') is also shown on the plot. We may exclude the region with $0.6 < s' < 0.8$, $0.25 < s < 0.9$ by this analysis at $\sqrt{s} = 0.5$ TeV. When the systematic error is not included, the shape of the plot is luminosity dependent, even for a luminosity as low as $L_{\mathrm{int}} \sim 10^3\,\mathrm{pb}^{-1}$ only the decoupling region ($s' = \sqrt{3/5}$) remains dark (not accessible) in this plot. At higher center of mass energies, different parameter regions can be constrained. The resonance regions deserve special attention at the ILC and CLIC energies, because the highest sensitivity to new physics is obtained in this region. Taking $s' = 0.5$, we can probe the Z_3 signal for the range of interest of $s = 0.5$–0.9 and $f = 0.5$–2.7 TeV at $\sqrt{s} = 0.5$ TeV and $L_{\mathrm{int}} = 100\,\mathrm{fb}^{-1}$. For the CLIC at $\sqrt{s} = 3$ TeV and $L_{\mathrm{int}} = 100\,\mathrm{fb}^{-1}$, and taking the mixing parameter $s' = 0.1$, we can probe the resonance peaks between the scale $f = 1$–3.7 TeV for almost the whole range of s. The extra gauge boson signals of LHM can be measured for almost the whole range of interest of

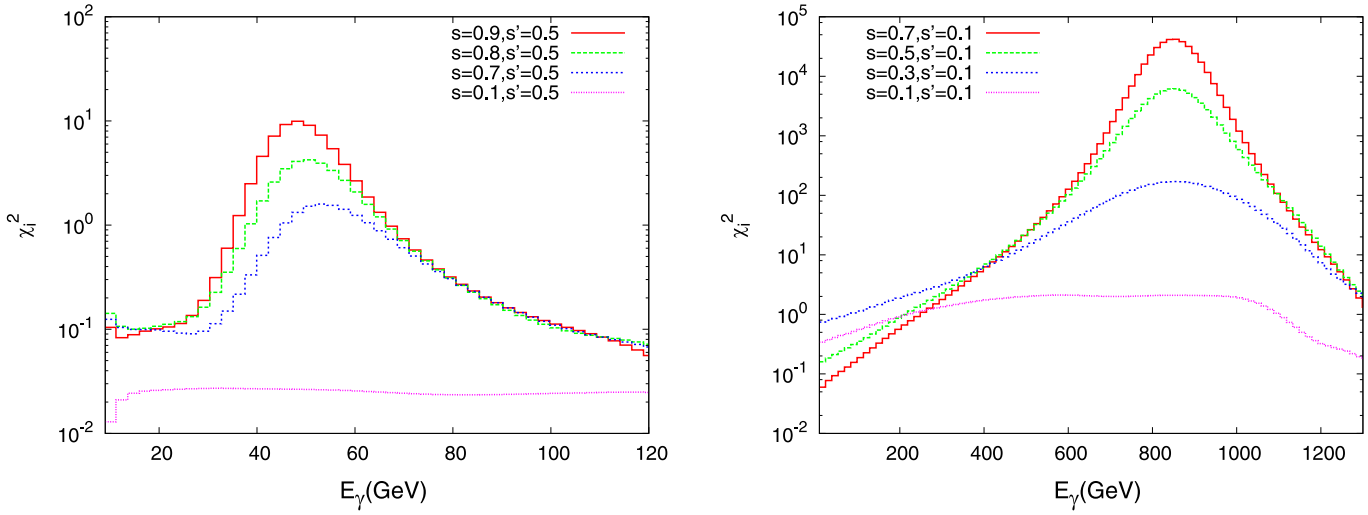

Fig. 9. The χ_i^2 distribution depending on the energy bin i for different LHM mixing parameters at ILC with $\sqrt{s} = 500$ GeV (*left*) and CLIC with $\sqrt{s} = 3$ TeV (*right*); here we assume $L_{\rm int} = 100\,{\rm fb}^{-1}$ and $v/f = 0.1$

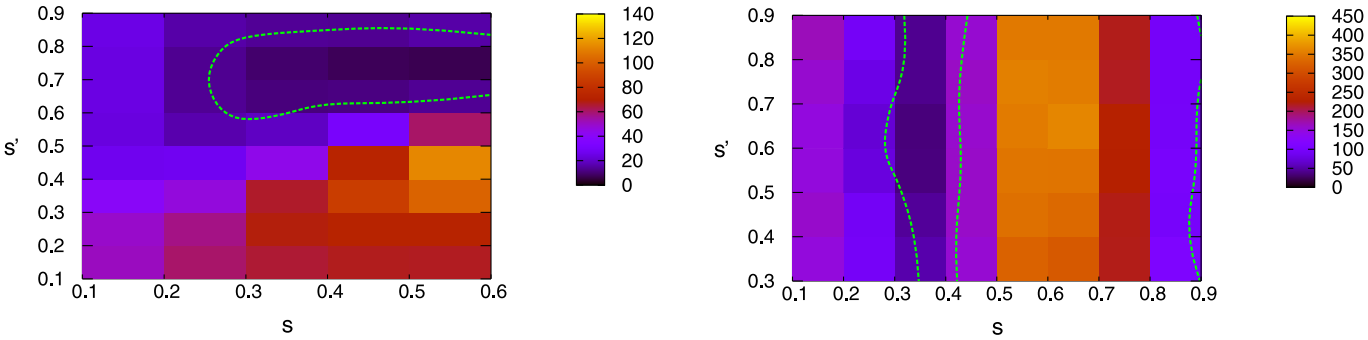

Fig. 10. The density plot and the contour lines with 95% C.L. for the search reach in the parameter space (s, s') with $v/f = 0.1$ (*left*) and $v/f = 0.07$ (*right*) at ILC (*left*) and CLIC (*right*) energies

s, s' except $0.3 < s < 0.4$ at CLIC with a projected luminosity $L_{\rm int} = 100\,{\rm fb}^{-1}$.

We can examine the specific behavior of the model in which the Z_2 and Z_3 decouples for $m_{Z_{2,3}} \to \infty$; in this way we can identify the contribution of $W_2^\pm$ to the reach of the search. At least their relative contributions can be compared. We find that for relatively small values of the scale f, the search reach is higher for lower values of s. For the point at which $s^2 = 0.5$, the minimal contribution comes from the charged heavy gauge boson, since the $W_2^\pm$ couplings reduce to that of the SM Z boson. If we take $s'^2 = 0.6$, the contributions will only come from the Z_2 and $W_2^\pm$ bosons.

4 Conclusions

In this work, we have studied the sensitivity of the process $e^+e^- \to \nu\bar{\nu}\gamma$ to the extra gauge bosons Z_2, Z_3 and $W_2^\pm$ in the framework of the little Higgs model. The search reach of the ILC (operating at $\sqrt{s} = 0.5$ TeV and $L_{\rm int} = 100\,{\rm fb}^{-1}$ for one year) and CLIC (when operating at $\sqrt{s} = 3$ TeV, and $L_{\rm int} = 100\,{\rm fb}^{-1}$) covers a wide range of parameter space in which this model is relevant to the hierarchy. For the parameter space where the resonances occur ($s' = 0.5(0.1)$) by scanning the parameter s, we can access the scale range $f = 0.5$–2.7 (1–3.7) TeV at $\sqrt{s} = 0.5(3)$ TeV, respectively. If the scale f is larger than $f \gtrsim 4$ TeV, sensitivity to the parameters of LHM could be reached with a detailed MC including detector and beam luminosity/energy uncertainty effects.

Finally, the ILC and CLIC with high luminosity have a high search potential for different regions of parameter space of the LHM. Analysis of the $e^+e^- \to \nu\bar{\nu}\gamma$ process can give valuable information about the LHM, and it can serve as a clean environment for a precise determination of its parameters. The measurements with small systematic errors are needed to have the desired sensitivity for the new physics parameters. Even for the cases in which the reach of the search for the extra gauge bosons in this process is not competitive with the potential of the LHC, the measurements at linear colliders can also provide detailed information on the extra gauge bosons that complements the results from the LHC.

Acknowledgements. The work of O.C. was supported in part by the State Planning Organization (DPT) under the grants no. DPT-2006K-120470 and in part by the Turkish Atomic Energy Authority (TAEA) under the grants no. VII-B.04.DPT.1.05.

References

1. N. Arkani-Hamed et al., JHEP **07**, 034 (2002)
2. N. Arkani-Hamed et al., JHEP **08**, 021 (2002)
3. T. Han et al., Phys. Rev. D **67**, 095 004 (2003)
4. M. Schmaltz, D.T. Smith, Ann. Rev. Nucl. Part. Sci. **55**, 229 (2005)
5. M. Perelstein, Prog. Part. Nucl. Phys. **58**, 247 (2007)
6. C. Csaki et al., Phys. Rev. D **67**, 115 002 (2003)
7. J.L. Hewett, F.J. Petriello, T.G. Rizzo, JHEP **0310**, 062 (2003)
8. M.C. Chen, S. Dawson, Phys. Rev. D **70**, 015 003 (2004)
9. C.X. Yue, W. Wang, Nucl. Phys. B **683**, 48 (2004)
10. W. Kilian, J. Reuter, Phys. Rev. D **70**, 015 004 (2004)
11. T. Han et al., Phys. Lett. B **563**, 191 (2003)
12. M. Blanke et al., hep-ph/0704.3329
13. M. Blanke et al., hep-ph/0703254
14. M. Blanke, A.J. Buras, hep-ph/0703117
15. M. Blanke et al., JHEP **0701**, 066 (2007)
16. M. Blanke et al., JHEP **0612**, 003 (2006)
17. P. Kai et al., hep-ph/07061358
18. X. Wang et al., hep-ph/0702164
19. F.M.L. de Almeida et al., hep-ph/0702137
20. X. Wang et al., hep-ph/0702064
21. J.A. Conley, J. Hewett, M.P. Le, Phys. Rev. D **72**, 115 014 (2005)
22. S. Godfrey, P. Kalyniak, B. Kamal, Phys. Rev. D **61**, 113 009 (2000)
23. G. Azuelos et al., Eur. Phys. J. C. **3952**, 13 (2005)
24. R. Brinkmann et al., TESLA technical design report, DESY-2001-011 (2001)
25. G.A. Loew, Report from the International Linear Collider Technical Review Committee, SLAC-PUB-10024 (2003)
26. http://www.linearcollider.org
27. The CLIC Study Team, R.W. Assmann et al., A 3 TeV e^+e^- linear collider based on CLIC technology, CERN 2000-008 (Geneva, 2000)
28. The CLIC Study Team, R.W. Assmann et al., CLIC contribution to the technical review committee on a 500 GeV e^+e^- linear collider, CERN-2003-007 (Geneva, 2003)
29. E. Accomando et al., Report of the CLIC physics working group, CERN-2004-005 (Geneva, 2004)
30. E. Accomando et al., hep-ph/0412251
31. E. Ma, J. Okada, Phys. Rev. D **8**, 4219 (1978)
32. CalcHEP/CompHEP Collaboration, A. Pukhov et al., hep-ph/9908288
33. CalcHEP/CompHEP Collaboration, A. Pukhov et al., hep-ph/0412191